Boletim da Sociedade Astronômica Brasileira, **33**, no. 1, 135-139


# Investigating Differences in the galaxy accretion history in Gaussian and non-Gaussian clusters:

## effects of different dynamical stages on member galaxy properties

V. M. Sampaio[1], R. R. de Carvalho[1], I. Ferreras[2], T. F. Laganá[1], A. L. B. Ribeiro[3] & S. B. Rembold[4]

[1] NAT - Universidade Cruzeiro do Sul / Universidade Cidade de São Paulo, 01506-000, SP, Brazil e-mail: vitorms999@gmail.com
[2] Instituto de Astrofísica de Canarias, Calle Ví a Láctea s/n,E38205, La Laguna, Tenerife, Spain
[3] Laboratório de Astrofísica Teórica e Observacional, Universidade Estadual de Santa Cruz, 45650-000, BA, Brazil
[4] Universidade Federal de Santa Maria, 97105-900, RS, Brazil

**Abstract.** We investigate the relation between the gaussianity of galaxy cluster velocity distribution and members galaxy properties. We use a sub sample of 177 clusters defined using the SDSS-DR7 Yang Catalog. Our sample is limited to $0.03 \leq z_{cluster} \leq 0.1$ and $\log(M_{halo}^{Cluster}/M_{\odot}) \geq 14$. Additionally, we divide clusters according to the shape of their velocity distribution into Gaussian (G, 143 systems) and non-Gaussian (NG, 34 systems) using the Hellinger Distance method. Comparison of the projected phase spaces (PPS) shows that the galaxy properties distribution is more mixed for NG in comparison to G systems. Using the relation between infall time and locus in the PPS, we provide a first estimate of the infall rate in NG clusters, namely these systems accreted $\sim 10^{11} M_{\odot}$ more stellar mass in the past $\sim$ 5 Gyr in comparison to G systems. Also, the relation between galaxy properties and infall time suggests that galaxies first infalling in NG systems are older and more metal rich than those infalling in G clusters. All these results suggests that G and NG clusters provide different environments to study galaxy evolution.

**Resumo.** Neste trabalho investigamos a relação entre a gaussianidade da distribuição de velocidade de aglomerados de galáxias e as propriedades dos sistemas membro. Nós utilizamos uma subamostra de 177 aglomerados derivados do catálogo de Yang. Nossa amostra é limitada à $0.03 \leq z_{cluster} \leq 0.1$ e a sistemas massivos, os quais possuem $\log(M_{halo}^{aglomerado} \geq 10^{14} M_{\odot})$. Além disso, dividimos os 177 sistemas de acordo com a forma de sua distribuição de velocidade entre Gaussianos (G, 143 sistemas) e não-Gaussianos (NG, 34 sistemas). Ao realizar uma comparação entre o espaço de fase projetado (EFP), encontramos distribuições das propriedades de galáxias membro mais "misturadas" no caso de aglomerados NG. Utilizamos também a relação entre local no EFP e tempo desde a acreção (infall time) para mostrar que sistemas NG acretaram nos ultimos 5 Giga-anos $\sim 10^{11} M_{\odot}$ mais massa estelar em comparação à sistemas G. Mais do que isso, um estudo das propriedades das galáxias membro em função do tempo desde a acreção mostra que as galáxias entrando em sistemas NG são mais velhas e possuem uma maior metalicidade do que sua contraparte em aglomerados G. Todos esses resultados indicam que aglomerados G e NG consistem em diferentes ambientes para o estudo da evolução de galáxias.

**Keywords.** Galaxies: clusters: general – Galaxies: evolution – Galaxies: general

## 1. Introduction

In the last decades, studies using wide field surveys have shown that galaxy evolution across the cosmic time is strongly dependent on environment. The Morphology-Density relation shows that early-type galaxies (ETGs) are mainly found in high density environments, while late-type systems (LTGs) dominate low density fields (Dressler 1980). This dichotomy is also seen in galaxy property distributions, for which galaxies in the field are bluer and more star-forming than those in clusters, for example (Wetzel, Tinker & Conroy 2012). This bimodal distribution results in three (two main and one intermediate) different regions in galaxy parameter space: 1) blue cloud – that contains blue, star forming galaxies; 2) red sequence – filled by "red and dead" galaxies evolving passively; and 3) green valley, that constitutes an intermediate region dominated by galaxies that are half-way to the full star formation quenching. Thus galaxy evolution is directly related to the mechanisms that drive galaxies from the blue cloud to the red sequence (and sometime the other way around!). When in low density fields, galaxy evolution is mostly driven by internal processes such as AGN and stellar feedback (e.g. Larson 1974; Bongiorno et al. 2016). However, when infalling into clusters, galaxies experience also additional quenching mechanisms driven by the high density environment. Even before crossing the cluster's virial radius, galaxies lose their hot gas (Strangulation, e.g. Balogh, Navarro & Morris 2000). After crossing the virial radius, the cluster's deep potential well may strip away galactic components such as gas, stars and even dark matter (tidal mass loss, e.g. Johnston, Sigurdsson & Hernquist 1999). Additionally, the intra cluster medium (ICM) is composed mainly by hot gas, which hidro-dynamically interacts with the infalling galaxy and cause a ram pressure that may remove galaxy's gas component (ram pressure stripping, e.g. Gunn & Gott 1972).

Additionally, star formation quenching in clusters is conditional on both galaxy and ICM properties. It is expected that environmental effects are more relevant for low mass galaxies evolution, while high mass systems rely mostly on internal mechanisms. However, the entirety of parameters that may affect galaxy evolution in clusters is not fully understood. For example, gravitationally bound objects are expected to reach a virialization state after a long enough time. The environment provided by relaxed system thus may be different from those that still unrelaxed. Substructure analysis in the optical (e.g. Dressler & Schectman 1988) and x-ray (Schuecker et al. 2001) further show that many clusters are not fully virialized. Yet, define the dynamical stage using only optical data is still challenging. Going back to statistical mechanics, one would expect the equilibrium state to be represented by a given velocity distribution. With this re-

gard, Ogorodnikov (1957) and Lynden-Bell (1967) suggest that the equilibrium state of gravitationally bound objects is characterized by a Maxwell-Boltzmann distribution. However, this result depends on several hypothesis, such as systems evolving in isolation. In real observations, galaxy clusters are not in isolation and, furthermore, we observationally only have access to projected along the line of sight (LOS) quantities. This makes the task of defining a equilibrium related distribution challenging. By using N-body simulations, Merral & Henriksen (2003) and Hansen et al. (2005) find that, after a perturbation, galaxy clusters reach the equilibrium when their velocity distribution have a Gaussian shape. This creates a separation between: 1) clusters that have their velocity distribution well fit by a gaussian distribution (G) – which are more prone to be in equilibrium; and 2) systems that have a non-Gaussian distribution (NG) – which are related to dinamycally perturbed systems.

Recently, different works investigate the differences between G and NG clusters: 1) NG clusters have an excess of star forming galaxies (Ribeiro, Lopes, & Trevisan 2010); 2) the stellar population parameters of virialized and infalling galaxies in NG clusters are not well separated as in G systems (Ribeiro et al. 2013); 3) there is evidence of a higher infall rate of pre-processed galaxies in NG clusters (Roberts & Parker 2017; de Carvalho et al. 2017); 4) NG clusters suffered their last major merger more recently than G systems (Roberts & Parker 2019). All these results corroborate to the fact that NG systems are related to perturbed systems. However, an important tool to understand system's dynamics is the phase space. Still, we are limited to the projected along the line of sight version of the phase space, which is called the projected phase space (PPS). It is built using the projected radial distance and velocity along the line of sight relative to the clustercentric coordinates in the x and y-axis, respectively. Also, it is common to normalize x and y-axis using virial radius and velocity dispersion, respectively, in order to enable comparison between different systems. Finally, the use of simulations relate location in the PPS with time since infall – defined as the time since the infalling galaxy has been experiencing the cluster environment (Rhee et al. 2017; Pasquali et al. 2019).

In this work, we use the PPS to further explore differences between G and NG clusters. We define a grid in order to explore different galaxy property distributions across the PPS of the two different galactic environments. Furthermore, we use the relation between location in the PPS and infall time to investigate the variation of galaxy properties as the time passes by. This also enable a first estimate of how much galaxies are infalling in NG systems in comparison to G clusters. This work is organized as follows: in Section 2 we define the sample, the catalogs used to retrieve galaxy properties and describe how we measure gaussianity; in section 3 we present our results; in sections 4 and 5 we present the discussion and conclusion, respectively. Throughout this work we adopt a flat ΛCDM cosmology with $[\Omega_M, \Omega_\Lambda, H_0] = [0.27, 0.73, 72\ \mathrm{km\ s^{-1} Mpc^{-1}}]$.

## 2. Data Selection and Methods

Our cluster sample is build upon the SDSS-DR7 version of the Yang Catalog (Yang et al. 2007), which is made by applying a halo finder algorithm (Yang et al. 2005) to the New York University - Value Added Galaxy Catalog (Blanton et al. 2005). However, we here make use of an updated version of the Yang Catalog described in de Carvalho et al. (2017) (dC17, hereon).

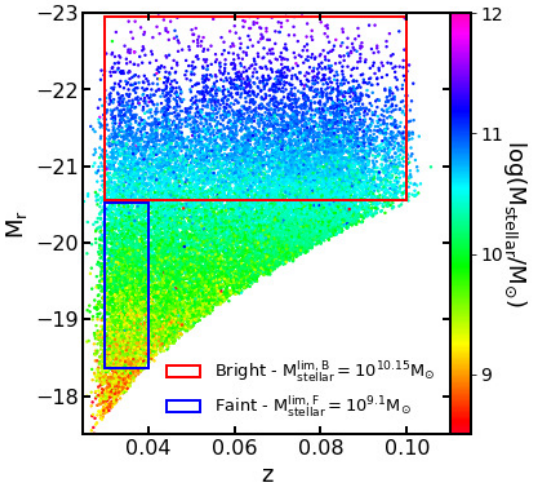


**Figure 1.** Galaxy distribution in the absolute magnitude ($M_r$) vs redshift (z) for our sample. The red rectangle define the bright regime, whereas the blue do the same for the faint regime. Galaxies are colored according to their stellar mass. In the legend we also show the completeness limit for each luminosity regime. Note that the y-axis is increasing to the bottom part.

### 2.1. Membership Selection

Members galaxy for each cluster are selected via Shiftgapper technique, which we describe next. First we query the SDSS-DR7 database for all galaxies within a projected distance of 3.5 Mpc and within the velocity range within $-4000 \leq v_{LOS} \leq +4000$ km, $s^{-1}$ from the clustercentric coordinates described in the original Yang catalog. We limit clustercentric redshift interval to $0.03 \leq z \leq 0.1$ and selected galaxies to r-band magnitudes brighter than 17.78, which is the survey spectroscopic completeness limit. These criteria guarantee that we are probing the luminosity function up to $M^\star + 1$. Selected galaxies are separated into radial bins with sizes guaranteeing at least 15 systems per bin. We then apply a gap technique in each bin that removes galaxies with a velocity gap greater than 1000 $km\ s^{-1}$ relative to the cluster mean velocity. This procedure is reiterated until there are no more removal of galaxies, which then defined the final member list for each cluster. Two reasons favors the use of the shiftgapper technique: 1) it is a method free of dynamical hypothesis; and 2) it is more permissive than the halo finder algorithm, which is impactful for galaxies in the outskirts of systems and may be relevant for galaxy evolution investigations.

Dynamical quantities such as velocity dispersion, virial mass and virial radius are estimated using the final member list for each cluster. Finally, we impose a minimum number of 20 galaxies within $R_{200}$, which results in 319 systems. Furthermore, member galaxies are separated into two different luminosity regimes: 1) Bright (B): $0.03 \leq z \leq 0.1$ and $M_r \leq -20.55 \sim M^\star + 1$ mag, where $M_r$ is the limiting absolute magnitude in the r-band; and 2) Faint (F): $0.03 \leq z \leq 0.04$ and $-20.55 < M_r \leq -18.40 \sim M^\star + 3$ mag. The redshift upper limit in the Faint sample corresponds to the spectroscopic completeness limit for $M_r = -18.40$ in the SDSS. Fig. 1 schematically shows the two luminosity regimes. The red rectangle denotes the bright regime, whereas the blue do the same for the faint regime.

### 2.2. Measuring the Gaussianity of the Cluster's Velocity Distribution

A pivotal part of this work is the separation between G and NG clusters. However, defining gaussianity is not a straightforward task in statistics. There are different approaches to define the shape of a distribution. For example, the Anderson-Darling normality test is one of the most employed methods to separate G and NG groups. However, its reliability depends on the number of member galaxies in each cluster. To avoid parametric methods, we define gaussianity using the Hellinger Distance method (Fadda et al. 1996). It is a method based on the Battacharya coefficient. For two discrete distributions, the distance between the two is defined as

$$\mathrm{HD}^2(\mathrm{P}_1, \mathrm{P}_2) = 2 \sum_{\mathrm{x}} \left[ \sqrt{p_1(x)} - \sqrt{p_2(x)} \right]^2, \quad (1)$$

where $p_1$ and $p_2$ are the two probability density functions (PDFs) and $x$ is a random variable. A characterization of the HD method done by dC17 shows that it is robust in distributions with a minimum number of 20 members within $R_{200}$, which translates to a mass cutoff. Namely, using the relation between $M_{200}$ and $N_{200}$ (where $N_{200}$ is the number of bright galaxies inside $R_{200}$), this translates to a minimum virial mass of $10^{14} M_\odot$ for our sample. We also only consider systems with at least 70% reliability on the gaussianity classification, which is measured with a bootstrap technique. This results in a sample of 143 and 34 G and NG clusters, respectively.

### 2.3. Galaxy Property Estimates

We retrieve galaxy properties from different sources. We briefly describe each one in the following. We select age, stellar metallicity ([Z/H], hereafter) and stellar mass ($M_{stellar}$) from the dC17. The estimates are obtained via the STARLIGHT Cid Fernandes et al. (2005) spectral fitting code, which uses a set of predefined single stellar population models (SSP) to fit the observed spectra. In this case, dC17 use the Medium resolution INT Library of Empirical Spectra (Sánchez-Blázquez et al. 2006), that has a spectral resolution $\sim$ 2.5 Å. The SSP grid has log(Age) steps of 0.2 dex from 0.07 to 14.2 Gyr and includes [Z/H] = $\{-1.71, -0.71, -0.38, 0.00, +0.20\}$. $M_{stellar}$ is first derived within the fiber and then corrected to the whole galaxy extent by computing the difference between fiber and model magnitudes in the z-band. Therefore, $M_{stellar}$ is given by:

$$\log(\mathrm{M_{stellar}}) = \log(\mathrm{M_{stellar}})' + 0.4\,(\mathrm{m_{fiber,z}} - \mathrm{m_{model,z}}). \quad (2)$$

Morphology is also relevant for galaxy evolution. Here we use the TType parameter to trace galaxy morphology. It was defined in order to classify S0 (lenticular) galaxies (de Vaucouleurs 1963). Each galaxy is assigned a number based on morphological visual classification. ETGs are denoted by TType<0, while TType>0 represents LTGs. We select TType estimates from the Dominguez-Sanchez catalog (Domínguez Sánchez et al. 2018), which uses deep learning algorithms based on Convolutional Neural Networks (CNN) to classify the morphology of SDSS galaxies.

Finally, we retrieve Star Formation Rates (SFR) from the Max Planck Institute for Astrophysics - John Hopkins University (MPA-JHU) catalog, which provides measurements for all SDSS-DR13 galaxies with reliable spectra. The available SFRs were computed using the $H_\alpha$ line luminosity measured within the spectroscopic fiber and corrected with photometry due to the aperture effect.

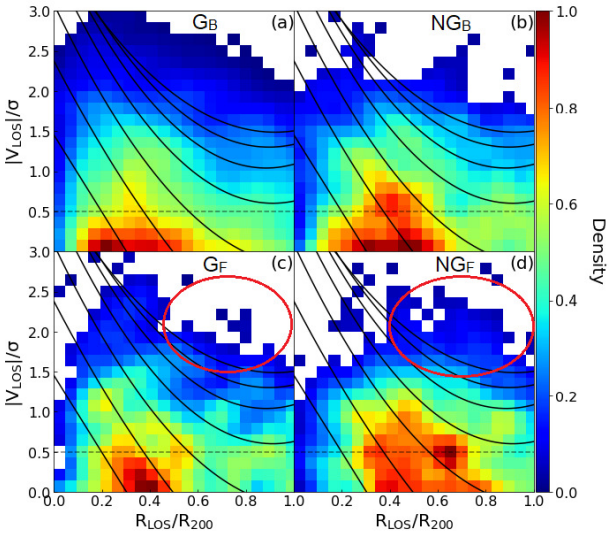


**Figure 2.** Normalized Kernel Smoothed Density of galaxies in the PPS of G (left) and NG (right) clusters. Top panels show the normalized density for bright galaxies, while the bottom panels do the same for faint galaxies. The red ellipses highlights the excess of faint galaxies in the PNZ 8 in the PPS of NG clusters.

## 3. Results

### 3.1. Galactic Density in the Projected Phase Space

We use the PPS to investigate further differences between G and NG clusters. Our analysis is done in a stacked version of the PPS following the prescription of Sampaio et al. (2021), which comprises galaxies in a given luminosity regime (B or F) and cluster class (G or NG). We also use the results presented in Pasquali et al. (2019), which relates location in the PPS with infall time through discrete zones (PNZs, hereafter) covering roughly from 1 (PNZ = 8, most outer region) to 5 (PNZ = 1, most inner region) Gyr. The mean infall time values for each region can be seen in their Table 1. However, it is noticeable that the PNZ 7 is quite narrow, which can impact the statistics of our analysis. We then decide to merge together regions 6 and 7 and adopt the respective mean infall time value. It is also important to highlight that the definition of PNZs are restricted to $1R_{200}$.

We first investigate differences regarding galaxy distribution in the PPS by dividing it into bins of $0.15|V_{LOS}|/\sigma \times 0.05 R_{LOS}/R_{200}$ to assure a good sampling of the PNZs, while adapting the bins to the aspect ratio of the diagram. Fig. 2 shows the normalized kernel smoothed density of galaxies in the PPS of G (left) and NG (right) clusters with respect to the two luminosity regimes (B - top and F - bottom). Comparison shows that, in both B and F regimes, the high density peak (red colors) in NG clusters extends towards higher velocities in comparison to G systems. Additionally, we find an excess of faint galaxies in the PNZ 8 (highlighted using a red ellipse) of NG clusters. It is expected that infalling galaxies have highly radial orbits, which are characterized by high velocities. Both our results indicate that there is an excess of infalling galaxies in NG clusters in comparison to G systems.

### 3.2. Galaxy Property Distributions

In the previous section we showed differences regarding galaxy distribution in the PPS of G and NG clusters. However, differences are also expected regarding galaxy properties distribution. Following a two component model (Carlberg et al. 1997), one

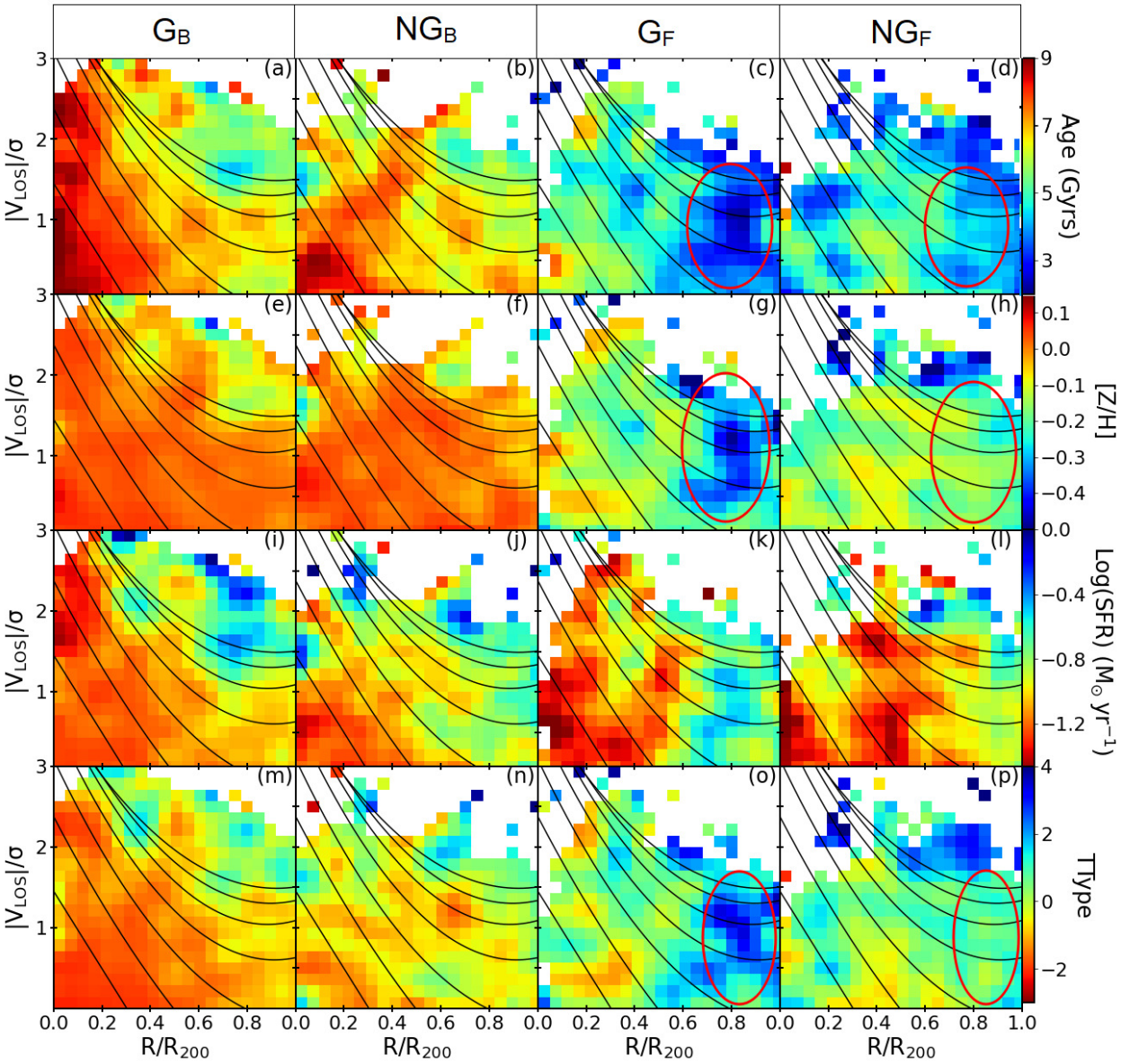


**Figure 3.** Age (first row), [Z/H] (second row), SFR (third row) and TType (last row) distribution in the PPS of G (first and third columns) and NG (second and fourth columns) clusters. Galaxies are divided according to luminosity regime. Black lines represent the PNZs and the red ellipses highlight noticeable differences between G and NG cluster member galaxy distributions.

would expect the inner part of cluster to be filled with red, older and more metal rich galaxies in comparison to the outskirt region. Deviation from this separation thus may be related to differences in the dynamical stage of such systems.

To investigate the galaxy property distributions, we use a similar procedure of Fig. 2. However, in this case each bin represent the median value of a given galaxy property. In Fig. 3 we show the distributions of Age, [Z/H], star formation rate (SFR) and TType for each luminosity regime and cluster class.

Exploring the distributions we find that NG clusters have more mixed distributions in comparison to G systems. Furthermore, we find that faint galaxy properties in the outskirt of NG systems is significantly different from its counterpart in G systems. Namely, galaxies in the outskirt of NG systems are older, more metal rich and have lower values of TType. This suggests that additionally to a higher infall rate in NG clusters, these system may be accreting mostly pre-processed galaxies, that already experienced part of their evolution before even entering the cluster environment.

### 3.3. Estimate of the Infall Rate

We can use the relation between location in the PPS and time since infall to derive a first estimate of the accretion rate in NG cluster in comparison to G systems. Differently from the previous analysis, here we consider the PPS for each cluster separately. In a first approximation, we calculate the sum of stellar mass in PNZ 8 (which is occupied mainly by galaxies with infall time $\sim 1.42$ Gyr – recent infallers) for each cluster and then take an average value for a given cluster class (G or NG) and luminosity regime (B or F). In the bright regime, NG clusters have an excess of stellar mass of $0.51 \times 10^{11}$ M$_\odot$ in PNZ 8, with respect to G clusters. In the faint regime, we also note NG clusters have an excess of $0.33 \times 10^{11}$M$_\odot$. Putting together the contributions of B and F galaxies, we find that NG clusters have an excess of $\sim 10^{11}$M$_\odot$ in the PNZ 8. This shows an excess of galaxies infalling in NG clusters.

A second estimate is derived by using not only the PNZ 8 but also the other PNZs. The mean infall rate ($\langle$IR$\rangle$) over all the

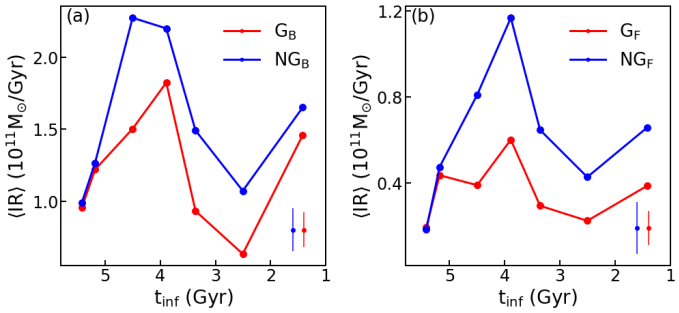


**Figure 4.** Mean infall rate of G (red) and NG (blue) clusters. We separate galaxies accordint to their luminosity into bright (left) and faint (right). The errorbars in the bottom right show the median error of each curve.

PNZs is calculated as follows: 1) sum the stellar mass within a single PNZ and divide it by the mean infall range of PNZ i - PNZ i-1; 2) take the average value for each PNZ for G or NG clusters and luminosity regime; and 3) these estimates provide, in first approximation, an infall history for G and NG clusters, which is shown in Fig. 4.

Comparison results in a mean difference of $\langle\langle IR\rangle_{NG} - \langle IR\rangle_G\rangle = 0.4 \times 10^{11} M_\odot$ and $0.3 \times 10^{11} M_\odot$ in the B and F regimes, respectively. By integrating the relations, suggests that NG clusters accreted $(1.5 \pm 0.8) \times 10^{12} M_\odot$ more stellar mass in the last $\sim 5$ Gyr than G systems. This is a first direct evidence of a higher infall rate in NG clusters.

## 4. Conclusion

In this work we explore differences between G and NG clusters from the PPS perspective. The main results are:

- in both bright and faint regimes, we find that galaxy distribution in the PPS of NG clusters show a high density peak that extends towards higher velocities. High velocity systems are expected to have highly radial orbits, which are characteristic of first infalling galaxies;
- in addition, we find that galaxy property distributions are also significantly different. Namely, we find more mixed distribution in the PPS of NG clusters in comparison to G systems. This properties mixture may be related to non-equilibrium, since virialized systems are expect to have a well defined separation between galaxy properties;
- by the way of the PPS, we define the mean infall rate, for which we find that NG clusters have accreted roughly $(1.5 \pm 0.8) \times 10^{12} M_\odot$ more stellar mass in the last $\sim 5$ Gyr than G systems.

We find that the most striking differences happen in the faint regime. This is in agreement with environmental effects being increasingly relevant for decreasing stellar mass. Furthermore, it reinforces that galaxy evolution also depends on host cluster properties. The differences we find suggest a higher infall rate in NG systems, which means that G and NG systems consist of different environments to study galaxy evolution. For further discussion, details and results check the full paper at: *https://arxiv.org/pdf/2103.03030.pdf*

*Acknowledgements.* RRdC and VMS thank T. S. Gonçalves for fruitful discussions on this topic. VMS acknowledges the FAPESP scholarship through the grant 2020/16243-3. RRdC aknowledges the financial support from FAPESP through the grant #2014/11156-4. TFL acknowledges financial support from FAPESP (2018/02626-8) and CNPq (306163/2019-5). IF acknowledges support from the Spanish Ministry of Science, Innovation and Universities (MCIU), through grant PID2019-104788GB-I00. ALBR thanks the support of CNPq, grant 311932/2017-7. S.B.R. acknowledges support from Conselho Nacional de Desenvolvimento Científico e Tecnológico – CNPq. This work was made possible thanks to a number of open-source software packages.

## References

Balogh M. L., Navarro J. F., Morris S. L., 2000, ApJ, 540, 113. doi:10.1086/309323
Blanton M. R., Schlegel D. J., Strauss M. A., Brinkmann J., Finkbeiner D., Fukugita M., Gunn J. E., et al., 2005, AJ, 129, 2562. doi:10.1086/429803
Bongiorno A., Schulze A., Merloni A., Zamorani G., Ilbert O., La Franca F., Peng Y., et al., 2016, A&A, 588, A78. doi:10.1051/0004-6361/201527436
Carlberg R. G., Yee H. K. C., Ellingson E., Morris S. L., Abraham R., Gravel P., Pritchet C. J., et al., 1997, ApJL, 476, L7. doi:10.1086/310497
de Carvalho R. R., Ribeiro A. L. B., Stalder D. H., Rosa R. R., Costa A. P., Moura T. C., 2017, AJ, 154, 96. doi:10.3847/1538-3881/aa7f2b
Cid Fernandes R., Mateus A., Sodré L., Stasińska G., Gomes J. M., 2005, MNRAS, 358, 363. doi:10.1111/j.1365-2966.2005.08752.x
Dressler A., 1980, ApJ, 236, 351. doi:10.1086/157753
Dressler A., Shectman S. A., 1988, AJ, 95, 985. doi:10.1086/114694
Domínguez Sánchez H., Huertas-Company M., Bernardi M., Tuccillo D., Fischer J. L., 2018, MNRAS, 476, 3661. doi:10.1093/mnras/sty338
Fadda D., Girardi M., Giuricin G., Mardirossian F., Mezzetti M., 1996, ApJ, 473, 670. doi:10.1086/178180
Gunn J. E., Gott J. R., 1972, ApJ, 176, 1. doi:10.1086/151605
Hansen S. H., Egli D., Hollenstein L., Salzmann C., 2005, NewA, 10, 379. doi:10.1016/j.newast.2005.01.005
Johnston K. V., Sigurdsson S., Hernquist L., 1999, MNRAS, 302, 771. doi:10.1046/j.1365-8711.1999.02200.x
Larson R. B., 1974, MNRAS, 169, 229. doi:10.1093/mnras/169.2.229
Merrall T. E. C., Henriksen R. N., 2003, ApJ, 595, 43. doi:10.1086/377249
Ogorodnikov K. F., 1957, SvA, 1, 748
Pasquali A., Smith R., Gallazzi A., De Lucia G., Zibetti S., Hirschmann M., Yi S. K., 2019, MNRAS, 484, 1702. doi:10.1093/mnras/sty3530
Ribeiro A. L. B., Lopes P. A. A., Trevisan M., 2010, MNRAS, 409, L124. doi:10.1111/j.1745-3933.2010.00962.x
Rhee J., Smith R., Choi H., Yi S. K., Jaffé Y., Candlish G., Sánchez-Jánssen R., 2017, ApJ, 843, 128. doi:10.3847/1538-4357/aa6d6c
Ribeiro A. L. B., de Carvalho R. R., Trevisan M., Capelato H. V., La Barbera F., Lopes P. A. A., Schilling A. C., 2013, MNRAS, 434, 784. doi:10.1093/mnras/stt1071
Roberts I. D., Parker L. C., 2017, MNRAS, 467, 3268. doi:10.1093/mnras/stx317
Roberts I. D., Parker L. C., 2019, MNRAS, 490, 773. doi:10.1093/mnras/stz2666
Sampaio V. M., de Carvalho R. R., Ferreras I., Laganá T. F., Ribeiro A. L. B., Rembold S. B., 2021, MNRAS, 503, 3065. doi:10.1093/mnras/stab673
Sánchez-Blázquez P., Peletier R. F., Jiménez-Vicente J., Cardiel N., Cenarro A. J., Falcón-Barroso J., Gorgas J., et al., 2006, MNRAS, 371, 703. doi:10.1111/j.1365-2966.2006.10699.x
Schuecker P., Böhringer H., Reiprich T. H., Feretti L., 2001, A&A, 378, 408. doi:10.1051/0004-6361:20011215
de Vaucouleurs G., 1963, ApJS, 8, 31. doi:10.1086/190084
Yang X., Mo H. J., van den Bosch F. C., Jing Y. P., 2005, MNRAS, 356, 1293. doi:10.1111/j.1365-2966.2005.08560.x
Yang X., Mo H. J., van den Bosch F. C., Pasquali A., Li C., Barden M., 2007, ApJ, 671, 153. doi:10.1086/522027
Wetzel A. R., Tinker J. L., Conroy C., 2012, MNRAS, 424, 232. doi:10.1111/j.1365-2966.2012.21188.x